Electronic Supplementary Material (ESI) for Journal of Materials Chemistry A.
This journal is © The Royal Society of Chemistry 2016

SUPPLEMENTARY INFORMATION

Sodium-ion storage performance of hierarchical-structured $(Co_{1/3}Fe_{2/3})Se_2$ nanofibers with fiber-in-tube nanostructures

Young Jun Hong, Jung Hyun Kim and Yun Chan Kang*

Department of Materials Science and Engineering, Korea University, Anam-dong, Seongbuk-gu, Seoul 136-713, Republic of Korea

E-mail: yckang@korea.ac.kr Fax: +82-2-928-3584; Tel: +82-2-3290-3268

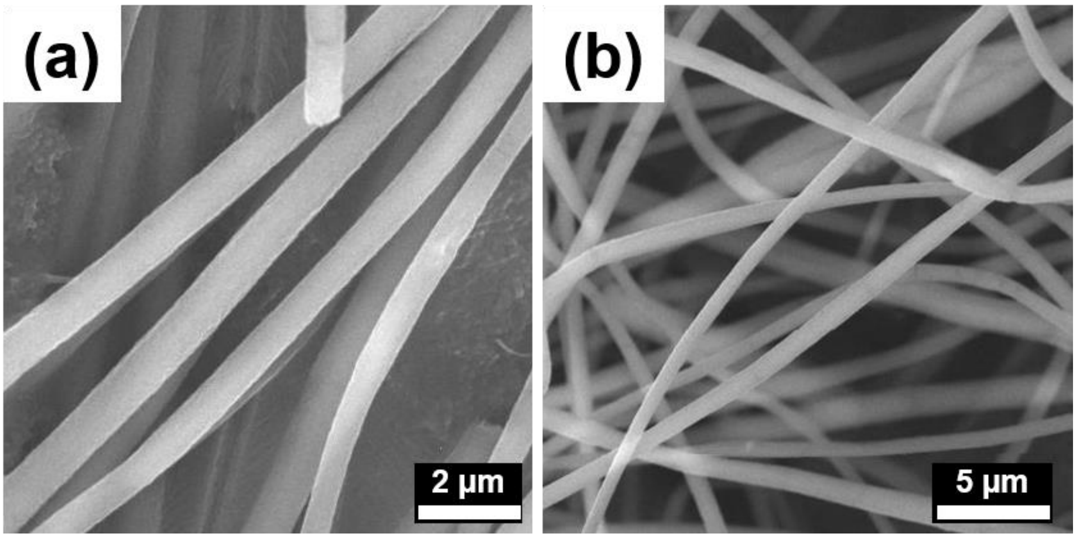

Fig. S1 Morphologies of the electrospun fibers.

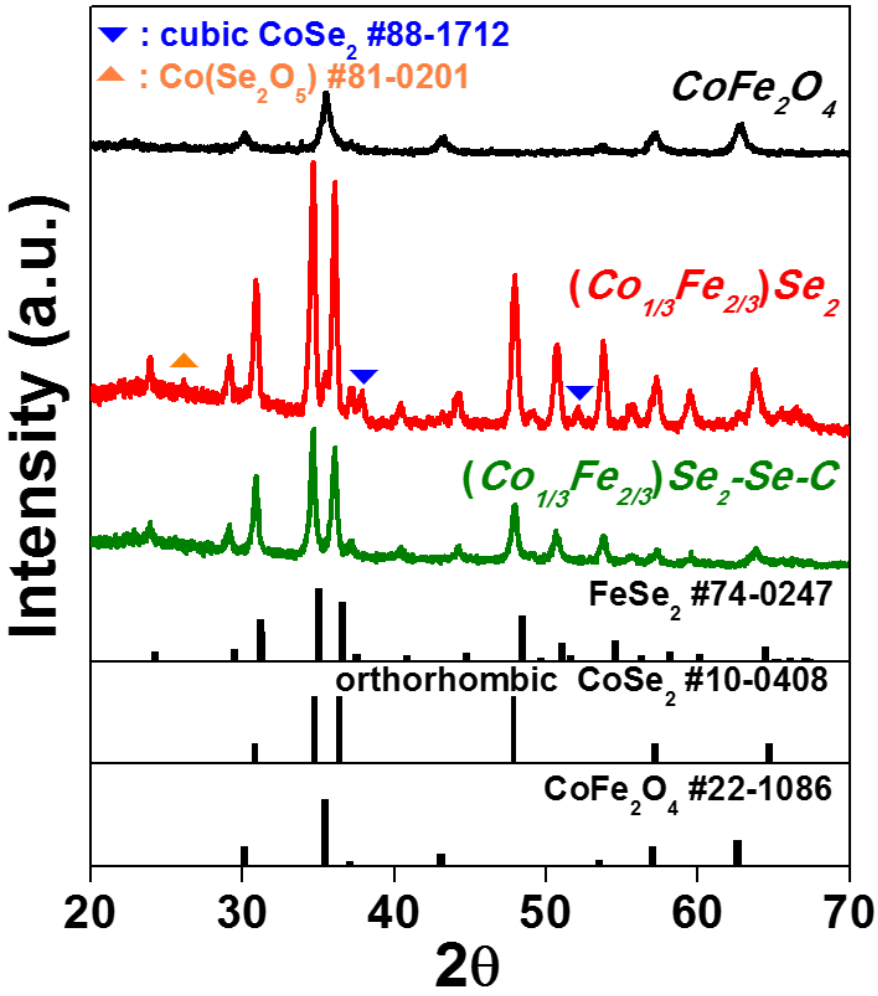

Fig. S2 XRD patterns of the $CoFe_2O_4$, $(Co_{1/3}Fe_{2/3})Se_2$, and $(Co_{1/3}Fe_{2/3})Se_2$-Se-C composite nanofibers.

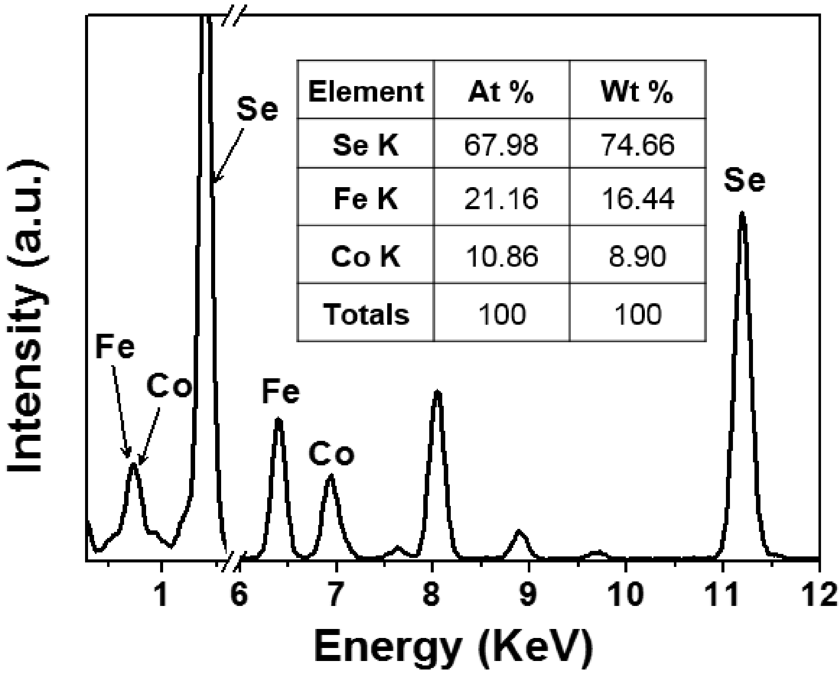

Fig. S3. EDAX spectrum and composition of the $(Co_{1/3}Fe_{2/3})Se_2$ nanofibers.

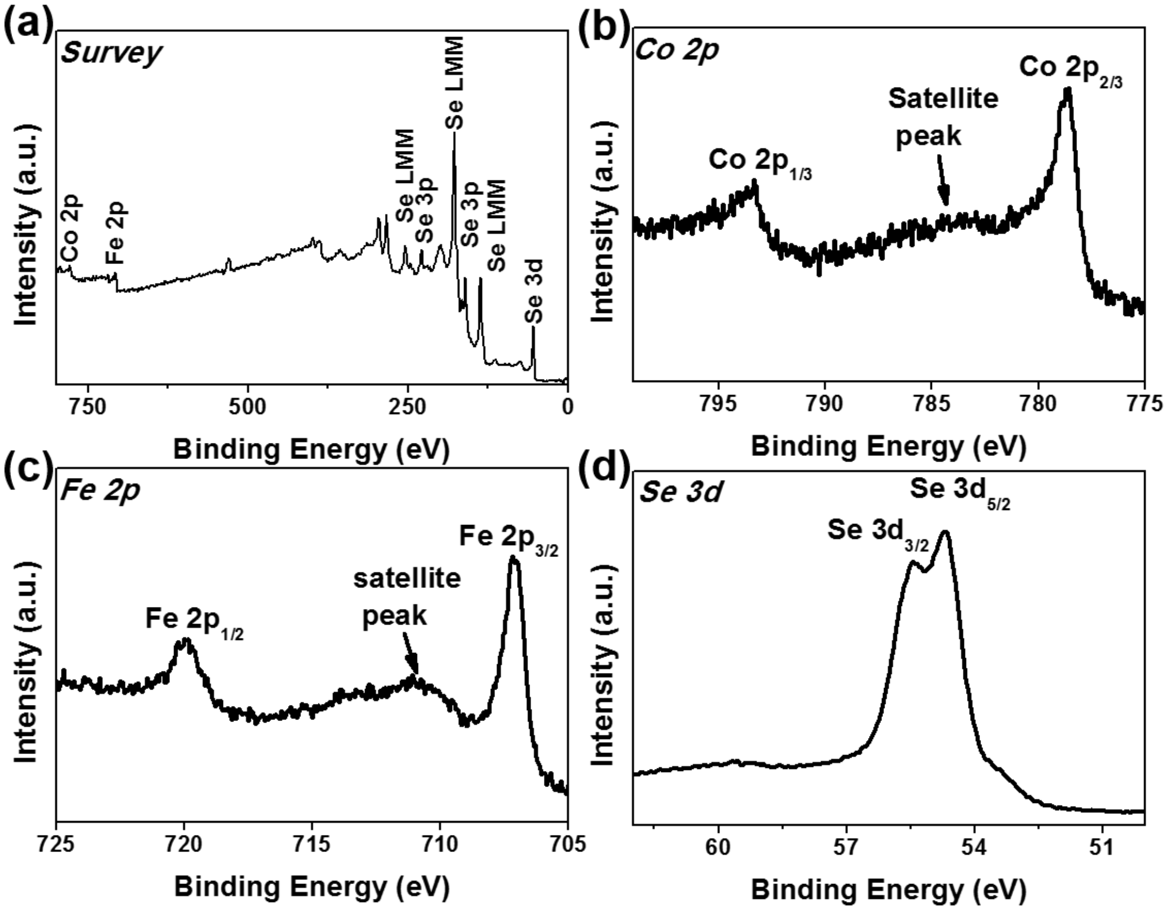

Fig. S4 XPS spectra of the hierarchical-structured $(Co_{1/3}Fe_{2/3})Se_2$ nanofibers: (a) survey scan, (b) XPS spectrum of Co 2*p*, (c) XPS spectrum of Fe 2*p*, (c) XPS spectrum of Se 2*d*.

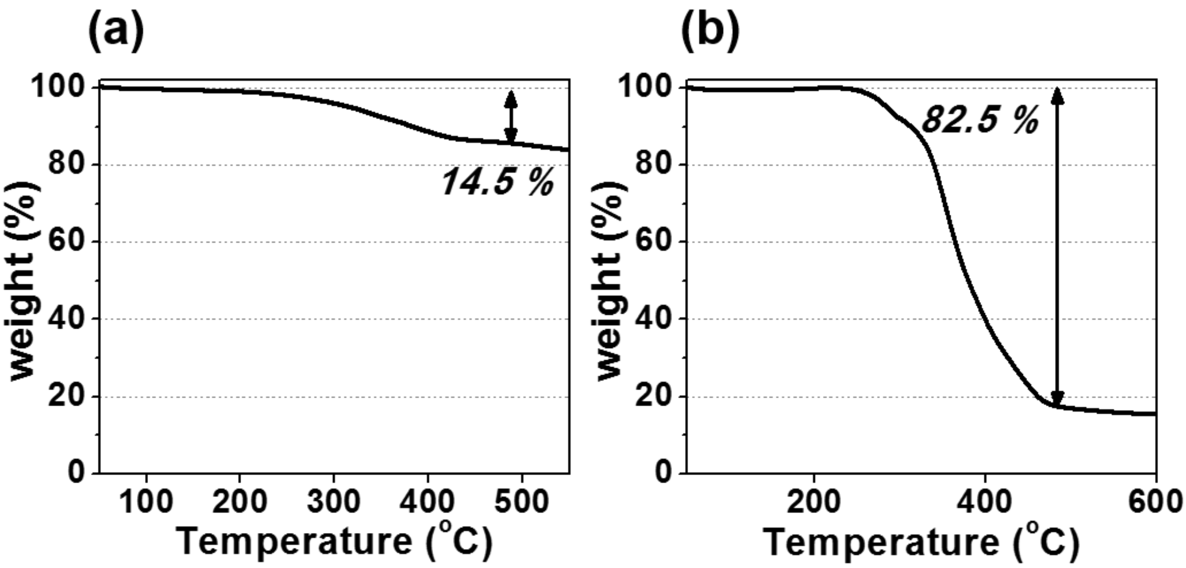

Fig. S5 The TG curves of the $(Co_{1/3}Fe_{2/3})Se_2$-Se-C composite nanofibers measured under (a) Ar and (b) air atmospheres.

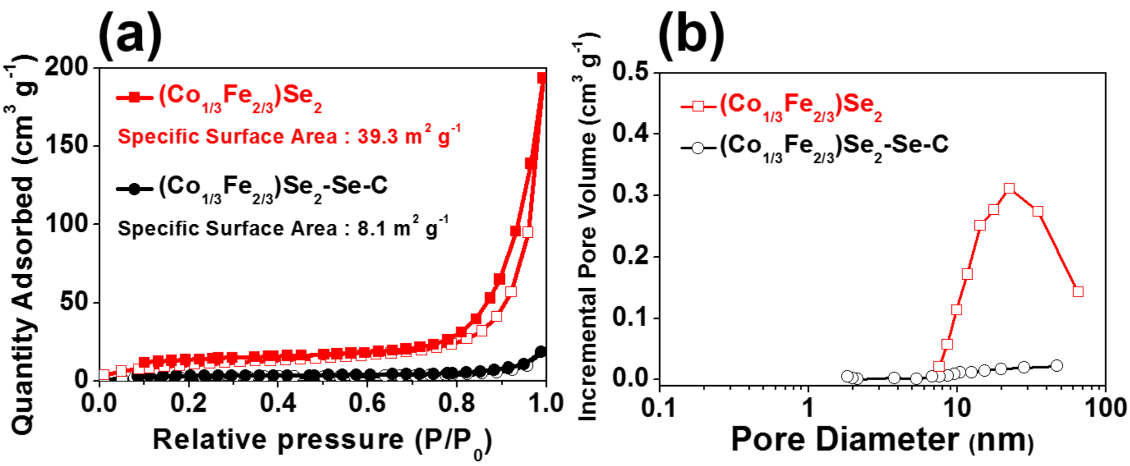

Fig. S6. N_2 adsorption and desorption isotherms and BJH pore size distributions of the $(Co_{1/3}Fe_{1/3})Se_2$ and $(Co_{1/3}Fe_{1/3})Se_2$-Se-C nanofibers.

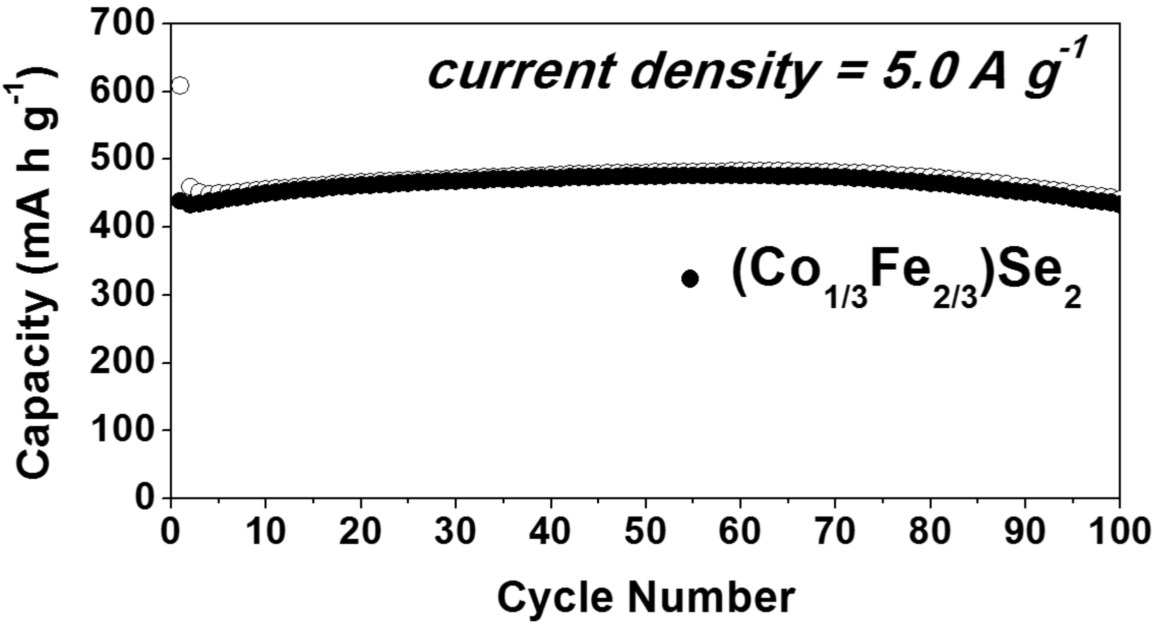

Fig. S7 The cycling performances of the hierarchical-structured ($Co_{1/3}Fe_{2/3}$)Se_2 nanofibers at a high current density of 5 A g^{-1}.

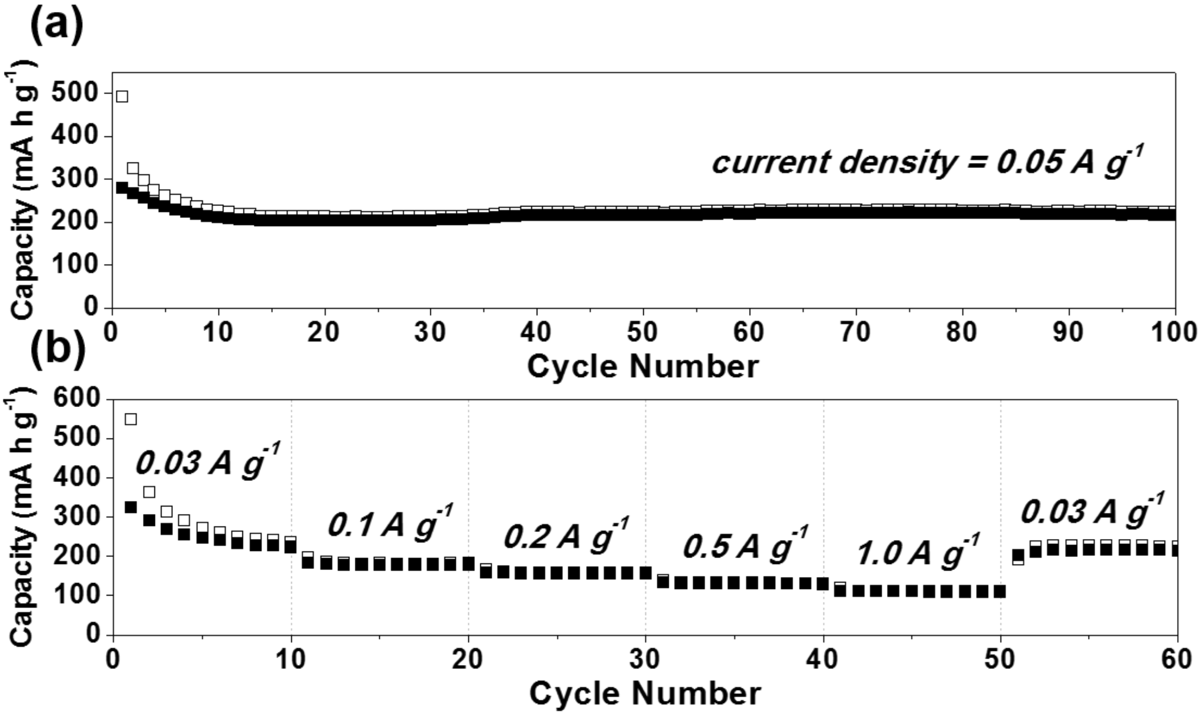

Fig. S8 The sodium-ion storage performances of the $CoFe_2O_4$ nanofibers with tube-in-tube structures: (a) cycling performances and (b) rate performances.

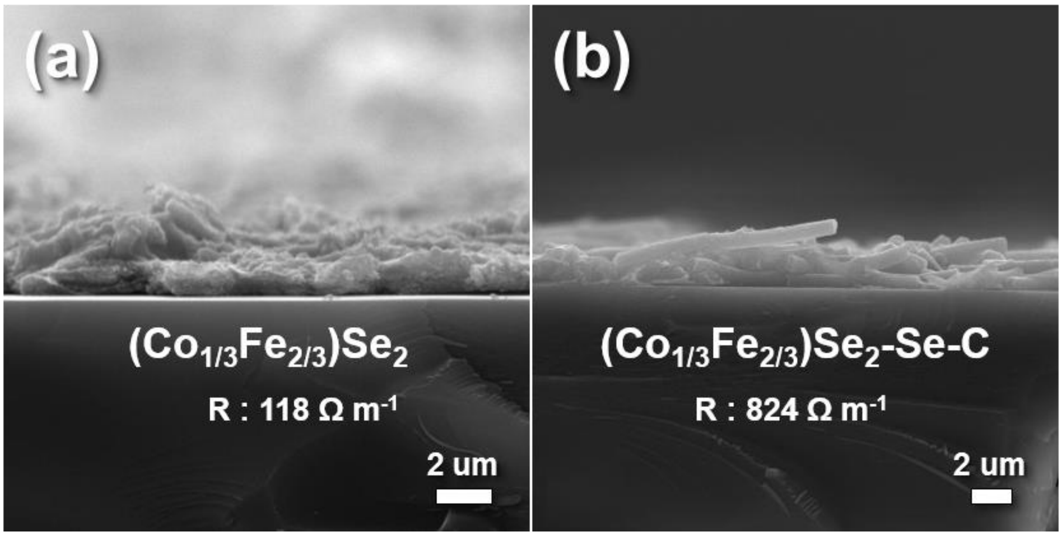

Fig. S9 SEM images of the (a) $(Co_{1/3}Fe_{2/3})Se_2$ and (b) $(Co_{1/3}Fe_{2/3})Se_2$-Se-C sheets formed on glass substrate.

Table S1. Sodium-ion storage properties of various metal chalcogenides and Sb materials.

metal chalcogenides & Sb materials	Synthesis	Electrochemical properties	Capacity retention	Ref
Cu_3P nanowire	In situ growth & phosphidation	134 mA h g^{-1} after 260 cycles at 1.0 A g^{-1}	~70 %	3
Tin phosphide	Ball milling	718 mA h g^{-1} after 50 cycles at 0.1 A g^{-1}	-	4
Flower-like hierarchical Cu_2NiSnS_4 - rGO	Hydrothermal method	321 mA h g^{-1} after 100 cycles at 0.05 A g^{-1}	-	5
Pyrite FeS_2	Hydrothermal method	~200 mA h g^{-1} after 20,000 cycles at 1.0 A g^{-1}	~90 %	13
		~170 mA h g^{-1} after 12,000 cycles at 20.0 A g^{-1}	-	
Vanadium sulfide on reduced graphene oxide layer	Hydrothermal method	~241 mA h g^{-1} after 50 cycles at 0.1 A g^{-1}	-	14
Nickel disulphide graphene nanosheets composite	Hydrothermal method	407 mA h g^{-1} after 200 cycles at 0.087 A g^{-1}	77 %	15
MnS hollow microsphere	Hydrothermal method	308 mA h g^{-1} after 125 cycles at 0.1 A g^{-1}	62 %	16
		118 mA h g^{-1} at 0.8 A g^{-1}	rate test	
Flower-like Sb_2S_3	Polyol reflux process	641 mA h g^{-1} after 100 cycles at 0.2 A g^{-1}	94 % (from the 50th cycle)	17
		554.6 mA h g^{-1} at 2.0 A g^{-1}	rate test	
MoS_2/Graphene composite	Hydrothermal method	~306 mA h g^{-1} after 100 cycles at 0.02 A g^{-1}	61.3 %	18
$FeSe_2$ microspheres	Hydrothermal method	372 mA h g^{-1} after 2000 cycles at 1.0 A g^{-1}	89 %	19
SnSe/carbon nanocomposite	Ball milling	325 mA h g^{-1} after 200 cycles at 0.5 A g^{-1}	72.5 %	22
SnSe alloy	Ball milling	707 mA h g^{-1} after 50 cycles at 0.143 A g^{-1}	-	23
		~350 mA h g^{-1} at 0.77 A g^{-1}	rate test	
$MoSe_2$ yolk–shell microsphere	Spray pyrolysis	433 mA h g^{-1} after 50 cycles at 0.2 A g^{-1}	99 % (from the 2nd cycle)	24
SnSe nanoplate	Spray pyrolysis	558 mA h g^{-1} after 50 cycles at 0.3 A g^{-1}	100 % (from the 2nd cycle)	25
		~221 mA h g^{-1} at 2.0 A g^{-1}	rate test	
$NiSe_2$-rGO-C composite nanofiber	Electrospinning	468 mA h g^{-1} after 100 cycles at 0.2 A g^{-1}	-	26
Graphitic carbon-coated $FeSe_2$	Electrospinning	412 mA h g^{-1} after 150 cycles at 1.0 A g^{-1}	82 % (from the 2nd cycle)	27
Ultrathin MoS_2 embedded in the carbon nanofiber	Electrospinning	484 mA h g^{-1} after 100 cycles at 1.0 A g^{-1}	-	28
		253 mA h g^{-1} after 100 cycles at 10.0 A g^{-1}		
$CoSe_x$-rGO composite	Spray pyrolysis	420 mA h g^{-1} after 50 cycles at 0.3 A g^{-1}	80 % (from the 2nd cycle)	29
Nanoporous-Sb	Melt-spun	574 mA h g^{-1} after 200 cycles at 0.1 A g^{-1}	-	48

Highly ordered Sb nanorod array	Nanoimprinted AAO templating technique	521 mA h g^{-1} after 250 cycles at 0.2 A g^{-1}	~84 %	49
Porous hollow Sb microspheres	Replacement reaction	617 mA h g^{-1} after 100 cycles at 0.1 A g^{-1}	97 %	50
		313 mA h g^{-1} at 3.2 A g^{-1}	rate test	
Sb/C fibers	Electrospinning	350 mA h g^{-1} after 300 cycles at 0.1 A g^{-1}	83 %	51
Sb–C nanofibers	Electrospinning	450 mA h g^{-1} after 400 cycles at 0.1 A g^{-1}	> 90 %	52
Monodisperse Sb nanocrystals	Colloidal synthesis	580 mA h g^{-1} after 100 cycles at 0.66 A g^{-1}	> 90 %	53
Sb/MWCNT nanocomposite	Wet milled synthesis	387 mA h g^{-1} after 120 cycles at 0.2 A g^{-1}	76 %	54
rGO/nano Sb composite	Reduction method	598 mA h g^{-1} after 50 cycles at 0.131 A g^{-1}	93 %	55
		100 mA h g^{-1} at 6.6 A g^{-1}	rate test	
Antimony/multilayer graphene hybrid	Confined vapor deposition method	405 mA h g^{-1} after 200 cycles at 0.1 A g^{-1}	90 %	56
Antimony hollow nanospheres	Galvanic replacementt	622.2 mA h g^{-1} after 50 cycles at 0.05 A g^{-1}	-	57
		315 mA h g^{-1} at 1.6 A g^{-1}	rate test	
Sb@C coaxial nanotubes	Thermal-reduction strategy	407 mA h g^{-1} after 240 cycles at 0.1 A g^{-1}	-	58
		240 mA h g^{-1} after 2000 cycles at 1.0 A g^{-1}	-	
Ultrafine Sb nanocrystals embedded in carbon microspheres	One-pot spray pyrolysis	372 mA h g^{-1} after 100 cycles at 0.3 A g^{-1}	90 % (from the 2nd cycle)	59
Hierarchical-structured $(Co_{1/3}Fe_{2/3})Se_2$ nanofiber	Electrospinning	512 mA h g^{-1} after 60 cycles at 0.3 A g^{-1}	100 % (from the 2nd cycle)	This study
		441 mA h g^{-1} after 100 cycles at 5.0 A g^{-1}	96 % (from the 2nd cycle)	